Decoupled Double Synchronous Reference Frame PLL for Power Converters Control

Pedro Rodríguez, *Member, IEEE*, Josep Pou, *Member, IEEE*, Joan Bergas, *Member, IEEE*, J. Ignacio Candela, *Member, IEEE*, Rolando P. Burgos, *Member, IEEE*, and Dushan Boroyevich, *Fellow, IEEE*

***Abstract*—This paper deals with a crucial aspect in the control of grid-connected power converters, i.e., the detection of the fundamental-frequency positive-sequence component of the utility voltage under unbalanced and distorted conditions. Specifically, it proposes a positive-sequence detector based on a new decoupled double synchronous reference frame phase-locked loop (DDSRF–PLL), which completely eliminates the detection errors of conventional synchronous reference frame PLL's (SRF–PLL). This is achieved by transforming both positive- and negative-sequence components of the utility voltage into the double SRF, from which a decoupling network is developed in order to cleanly extract and separate the positive- and negative-sequence components. The resultant DDSRF–PLL conducts then to a fast, precise, and robust positive-sequence voltage detection even under unbalanced and distorted grid conditions. The paper presents a detailed description and derivation of the proposed detection method, together with an extensive evaluation using simulation and experimental results from a digital signal processor-based laboratory prototype in order to verify and validate the excellent performance achieved by the DDSRF–PLL.**

***Index Terms*—Grid-connected converters, phase locked loop (PLL), positive sequence signals detection, synchronous reference frame (SRF).**

I. Introduction

ONE of the most important aspects to consider in the control of grid-connected power converters is the proper synchronization with the utility voltages. Specifically, the detection of the positive-sequence voltage component at fundamental frequency is essential for the control of distributed generation and storage systems, flexible ac transmission systems (FACTS), power line conditioners and uninterruptible power supplies (UPS) [1], [2]. The magnitude and angle of the positive-sequence voltage is used for the synchronization of the converter output variables, power flux calculations, or for the transformation of state variables into rotating reference frames [3]–[5]. Regardless of the technique used in the system detection, the amplitude and the phase of the positive-sequence component must be fast and accurately obtained, even if the utility voltage is distorted and unbalanced.

There are two main approaches to detect the positive sequence component of the utility voltage. The first one assumes that the frequency of the utility is a constant and well-known magnitude, and is usually based on 1) instantaneous symmetrical components (ISC) [6], 2) on space vector filters (SVF) [7], or on 3) the recursive weighted least-square estimation algorithm (WLSE) [8]. The second approach assumes that the utility frequency is not constant, and uses closed-loop adaptive methods in order to render the detection algorithm insensitive to input frequency variations. In this sense, a frequency update algorithm can be used in the WLSE-based approach [9]. This method however exhibits long transient time intervals in the detection of frequency changes. The most extended technique used for frequency-insensitive positive-sequence detection is the three-phase phase locked loop (PLL) based on the synchronous reference frame (SRF–PLL) [10], although alternative structures are also possible [11]. A discussion on the behavior of the SRF-PLL under unbalanced grid conditions will be performed in Section II. Another possibility is to use some kind of enhanced single-phase PLL for each phase of the system [12], [13], allowing the estimation of frequency and in-phase and quadrature-phase waveforms for each of the phase voltages. These phase voltages and their respective 90° shifted versions can be used by the ISC method in order to detect the positive-sequence voltages of the three-phase system [14]. This improved version of the ISC approach uses an additional single-phase PLL to estimate the phase-angle of the detected positive-sequence voltage. Although this four-independent single-phase PLL-based technique offers good results in the estimation of the positive-sequence component in unbalanced power systems [15], some features can be improved by replacing the single-phase PLLs by an enhanced three-phase PLL structure.

This work presents an alternative detection method to be used in unbalanced power networks, namely the decoupled double synchronous reference frame PLL (DDSRF-PLL). The proposed technique defines an unbalanced voltage vector, consisting of both positive- and negative-sequence components, and expresses it on the double synchronous reference frame in order to detect the positive-sequence component [17], [18]. This is accomplished by studying the relationships between the transformed signals on the DSRF-axes, which combined with the design of a proper decoupling system enables a fast and accurate phase and amplitude detection of the utility voltage positive-sequence component under unbalanced utility conditions.

Manuscript received November 29, 2005; revised June 19, 2006. This paper was presented at IEEE PESC'05, Recife, Brazil, June 12–16, 2005. This work was supported by the Ministerio de Ciencia y Tecnologia of Spain under Grant PR2006-0411, Project ENE2004-07881-C03-02, the Engineering Research Center Shared Facilities supported by the National Science Foundation under NSF Award EEC-9731677, and by the CPES Industry Partnership Program. Recommended for publication by Associate Editor F. Blaabjerg.

P. Rodríguez, J. Bergas, and J. I. Candela are with the Department of Electrical Engineering, Technical University of Catalonia (UPC), Terrassa 08222, Spain (e-mail: prodriguez@ee.upc.edu).

J. Pou is with the Department of Electronic Engineering, Technical University of Catalonia (UPC), Terrassa 08222, Spain.

R. P. Burgos and D. Boroyevich are with the Center for Power Electronics Systems (CPES), The Bradley Department of Electrical and Computer Engineering, Virginia Polytechnic Institute and State University (Virginia Tech), Blacksburg, VA 24061 USA.

Digital Object Identifier 10.1109/TPEL.2006.890000

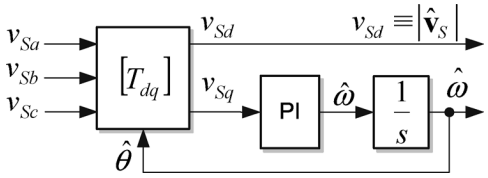

Fig. 1. Basic block diagram of the SRF-PLL.

II. Conventional SRF-PLL Under Unbalanced Grid Conditions

In the conventional SRF-PLL, the three-phase voltage vector is translated from the abc natural reference frame to the dq rotating reference frame by using Park's transformation $[T_{dq}]$ as shown in Fig. 1. The angular position of this dq reference frame is controlled by a feedback loop which regulates the q component to zero. Therefore in steady-state, the d component depicts the voltage vector amplitude and its phase is determined by the output of the feedback loop.

Under ideal utility conditions, i.e., neither harmonic distortion nor unbalance, a high band-width of the SRF-PLL feedback loop yields a fast and precise detection of the phase and amplitude of the utility voltage vector. In case the utility voltage is distorted with high-order harmonics, the SRF-PLL can operate satisfactorily if its bandwidth is reduced in order to reject and cancel out the effect of these harmonics on the output. It will be evinced in the following however that the PLL bandwidth reduction is not an acceptable solution in the presence of unbalanced grid voltages.

In unbalanced grid operating conditions (without voltage harmonics), the phase voltages V_{Si} with $i \in \{a, b, c\}$ can be generally expressed as

$$v_{Si} = V_S^{+1} \cos\left(\omega t - k\frac{2\pi}{3}\right) + V_S^{-1} \cos\left(-\omega t - k\frac{2\pi}{3} + \phi^{-1}\right) + V_S^0 \cos(\omega t + \phi^0) \quad (1)$$

where superscripts $+1$, -1 and 0 define the coefficients for the positive, negative and zero sequence components, and k takes values k =0, 1, 2 for $i = a, b, c$ respectively.

Using the non-normalized Clarke transformation, the utility voltage vector is given by

$$v_{S\,(\alpha\beta\gamma)} = \begin{bmatrix} v_{S\alpha} \\ v_{S\beta} \\ v_{S\gamma} \end{bmatrix}^T = [T_{\alpha\beta\gamma}] \begin{bmatrix} v_{Sa} \\ v_{Sb} \\ v_{Sc} \end{bmatrix}$$
$$\text{where} \quad [T_{\alpha\beta\gamma}] = \frac{2}{3} \begin{bmatrix} 1 & -\frac{1}{2} & -\frac{1}{2} \\ 0 & \frac{\sqrt{3}}{2} & -\frac{\sqrt{3}}{2} \\ \frac{1}{2} & \frac{1}{2} & \frac{1}{2} \end{bmatrix}. \quad (2)$$

Then, neglecting the zero-sequence component, the voltage vector in the $\alpha\beta$ plane is given by (3), where the positive sequence voltage component is supposed as the phase origin

$$\begin{aligned} v_{S\,(\alpha\beta)} &= \begin{bmatrix} v_{S\alpha} \\ v_{S\beta} \end{bmatrix} \\ &= v_{S\,(\alpha\beta)}^{+1} + v_{S\,(\alpha\beta)}^{-1} \\ &= V_S^{+1} \begin{bmatrix} \cos(\omega t) \\ \sin(\omega t) \end{bmatrix} + V_S^{-1} \begin{bmatrix} \cos(-\omega t + \phi^{-1}) \\ \sin(-\omega t + \phi^{-1}) \end{bmatrix}. \end{aligned} \quad (3)$$

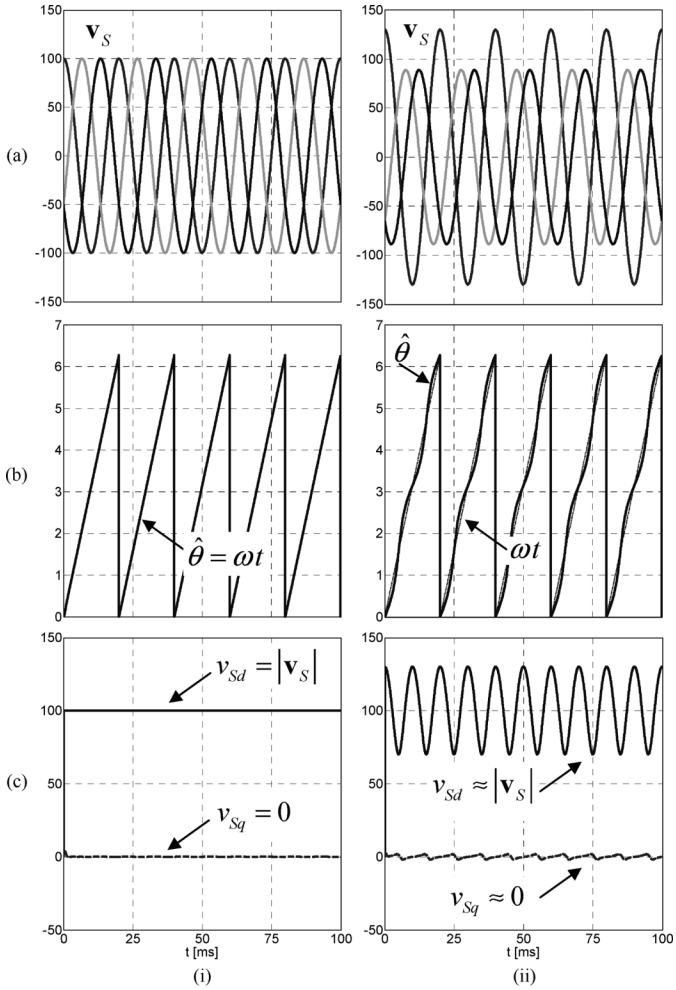

Fig. 2. Response of the SRF-PLL with high bandwidth under i) balanced and ii) unbalanced conditions. (a) Utility voltage [V], (b) Detected phase angle [rad], and (c) SRF axes voltage [V].

In (3), it is clear that v_S consists of two sub-vectors: v_S^{+1}, rotating with a positive angular frequency ω, and v_S^{-1}, rotating with a negative angular frequency $-\omega$. The amplitude and angular position of the voltage vector in (3) are, respectively, by (4a) and (4b), where it is clear that the voltage vector has neither constant magnitude nor constant rotational frequency under unbalanced grid conditions

$$|v_S| = \sqrt{\left(V_S^{+1}\right)^2 + \left(V_S^{-1}\right)^2 + 2V_S^{+1}V_S^{-1}\cos(-2\omega t + \phi^{-1})} \quad (4a)$$

$$\theta = \omega t + \tan^{-1}\left(\frac{V_S^{-1}\sin(-2\omega t + \phi^{-1})}{V_S^{+1} + V_S^{-1}\cos(-2\omega t + \phi^{-1})}\right). \quad (4b)$$

Fig. 2 shows the response of the SRF-PLL under balanced/unbalanced conditions when a high bandwidth is set for the control loop. The unbalanced utility voltage shown in Fig. 2(a,ii) is characterized by $V_S^{+1} = 100$ V, $V_S^{-1} = 30$ V $\phi^{+1} = \phi^{-1} = 0$ rad, and $\omega = 2\pi$ 50 rad/s. The parameters of the SRF-PLL are $k_p =$ 44,42 and $k_i = 9.87 \cdot 10^4$. A small-signal analysis justifying the selection of k_p and k_i is reported in [16]–[18] and briefly revised at then end of Section VI. As observed, the high bandwidth

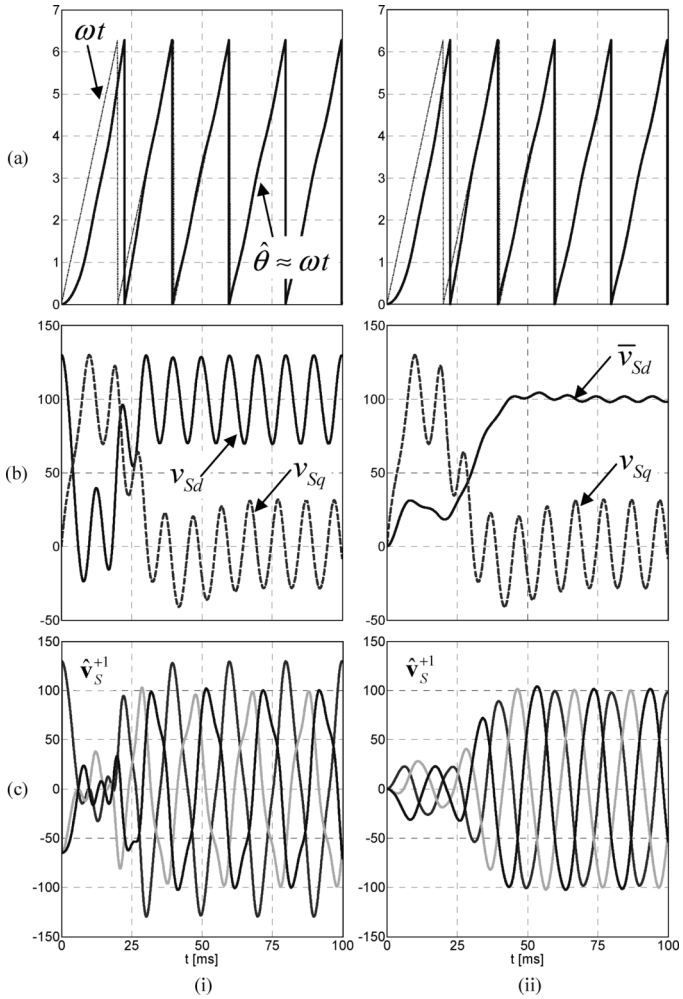

Fig. 3. Response of the SRF-PLL under unbalanced conditions with (i) low bandwidth and (ii) applying a second order low-pass filter to v_{Sd}. (a) Detected phase angle [rad]. (b) SRF axes voltage [V]. (c) Detected positive-sequence voltage [V].

achieves a nearly zero q-axis voltage ($v_{Sq} \approx 0$), even under unbalanced conditions. Consequently v_{Sd} and $\hat{\theta}$ are indeed given by (4a) and (4b), respectively, which implies that the amplitude and phase angle of the positive-sequence component cannot be precisely determined by simple filtering of these signals.

To achieve a better estimation of the phase angle of the positive-sequence voltage component the control-loop bandwidth can be reduced in order to force the appearance in v_{Sq} of the double frequency oscillation term shown in 4(b) [17], [18]. This is observed in column i) of Fig. 3, which shows the response of the SRF-PLL when the control-loop is detuned using $k_p = 1.78$ and $k_i = 157.9$, and the utility is unbalanced with the voltages depicted in Fig. 2. Under such conditions, it can be assumed that

$$v_{Sd} \approx V_S^{+1} + V_S^{-1}\cos(-2\omega t + \phi^{-1}) \tag{5a}$$

$$\theta \approx \omega t. \tag{5b}$$

From (5), the reconstruction of the positive-sequence component of the utility voltage could be tried, but its results would be poor as depicted in Fig. 3(c,i). Nonetheless, the mean value of v_{Sd} is very close to the amplitude of the positive sequence voltage component. Therefore, by using a simple low-pass filter the mean value of v_{Sd} may be extracted and by doing so estimate the amplitude of the positive-sequence voltage component. The plots of column (ii) in Fig. 3 show the response of the detuned SRF-PLL when a second-order low-pass Butterworth filter is applied to v_{Sd}, with a cut-off frequency of $\omega_c = 2\pi$ 25 rad/s. This figure shows that although the SRF-PLL response has been improved, this technique suffers from three critical limitations: 1) only an approximation but not the true amplitude and phase angle of the positive-sequence component are detected; 2) the detected positive-sequence voltages are distorted and unbalanced; and 3) the dynamic response of the system is significantly reduced [16]. Therefore, in applications requiring high accuracy and a good dynamic response even under unbalanced voltages, e.g., dynamic voltage restorers (DVR), the conventional SFR–PLL technique does not represent the most appropriate solution for the control of this type of power converters.

III. Unbalanced Voltage Vector on the DSRF

The detection method proposed in this paper uses a DSRF composed of two rotating reference axes: dq^{+1}, rotating with the positive direction and whose angular position is $\hat{\theta}$, and dq^{-1}, rotating with the negative direction and whose angular position is $-\hat{\theta}$. Then, the voltage vector v_S may be expressed on the DSRF yielding

$$\begin{aligned} v_{S_{(dq^{+1})}} &= \begin{bmatrix} v_{Sd^{+1}} \\ v_{Sq^{+1}} \end{bmatrix} \\ &= [T_{dq^{+1}}] \cdot v_{S_{(\alpha\beta)}} \\ &= V_S^{+1}\begin{bmatrix} \cos(\omega t - \hat{\theta}) \\ \sin(\omega t - \hat{\theta}) \end{bmatrix} \\ &\quad + V_S^{-1}\begin{bmatrix} \cos(-\omega t + \phi^{-1} - \hat{\theta}) \\ \sin(-\omega t + \phi^{-1} - \hat{\theta}) \end{bmatrix} \end{aligned} \tag{6a}$$

$$\begin{aligned} v_{S_{(dq^{-1})}} &= \begin{bmatrix} v_{Sd^{-1}} \\ v_{Sq^{-1}} \end{bmatrix} \\ &= [T_{dq^{-1}}] \cdot v_{S_{(\alpha\beta)}} \\ &= V_S^{+1}\begin{bmatrix} \cos(\omega t + \hat{\theta}) \\ \sin(\omega t + \hat{\theta}) \end{bmatrix} \\ &\quad + V_S^{-1}\begin{bmatrix} \cos(-\omega t + \phi^{-1} + \hat{\theta}) \\ \sin(-\omega t + \phi^{-1} + \hat{\theta}) \end{bmatrix} \end{aligned} \tag{6b}$$

where

$$[T_{dq^{+1}}] = [T_{dq^{-1}}]^T = \begin{bmatrix} \cos(\hat{\theta}) & \sin(\hat{\theta}) \\ -\sin(\hat{\theta}) & \cos(\hat{\theta}) \end{bmatrix} \tag{7}$$

Fig. 4 shows the voltage vectors and the reference frames for (6).

Using a PLL structure similar to the one shown in Fig. 1, and adjusting properly its control parameters, it is possible to achieve $\hat{\theta} \approx \omega t$. As mentioned earlier, the selection of this PLL control parameters is based on a small-signal analysis [16] in which it is assumed that $\sin(\omega t - \hat{\theta}) \approx (\omega t - \hat{\theta})$, $\cos(\omega t -$

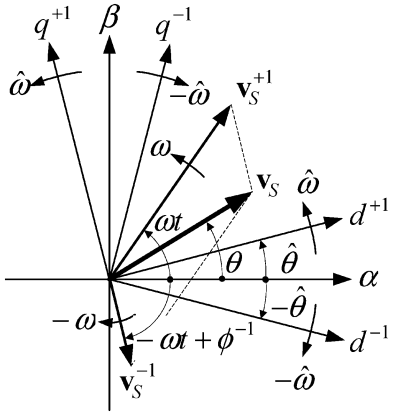

Fig. 4. Voltage vectors and axes of the DSRF.

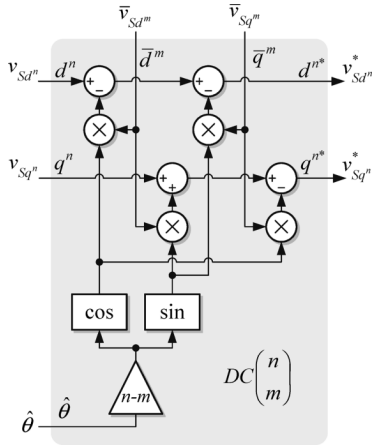

Fig. 5. Decoupling cell for canceling the effect of v_S^m on the dq^n frame signals.

$\hat{\theta}) \approx 1-((\omega t-\hat{\theta})^2/2)$, and $(-\omega t-\hat{\theta}) \approx -2\omega t$. Under such conditions (6) can be linearized and rewritten as

$$v_{S\atop(dq^{+1})} \approx V_S^{+1}\begin{bmatrix}1-\left((\omega t-\hat{\theta})^2/2\right)\\ \omega t-\hat{\theta}\end{bmatrix} + V_S^{-1}\begin{bmatrix}\cos(-2\omega t+\phi^{-1})\\ \sin(-2\omega t+\phi^{-1})\end{bmatrix} \tag{8a}$$

$$v_{S\atop(dq^{-1})} \approx V_S^{+1}\begin{bmatrix}\cos(2\omega t)\\ \sin(2\omega t)\end{bmatrix} + V_S^{-1}\begin{bmatrix}\cos(\phi^{-1})\\ \sin(\phi^{-1})\end{bmatrix}. \tag{8b}$$

In (8), the constant values on the dq^{+1} and the dq^{-1} axes correspond to the amplitude of v_S^{+1} and v_S^{-1}, while the oscillations at 2ω correspond to the coupling between axes appearing as a consequence of the vectors rotating in opposite direction. These oscillations may be simply considered perturbations in the detection of v_S^{+1} and v_S^{-1}; however the attenuation of these oscillations by means of conventional filtering techniques gives rise to the drawbacks exposed previously in Section II, hence this is not desirable [16]–[18]. In order to cancel out these oscillations, this paper proposes the usage of a decoupling network (DN) instead, capable of obtaining accurate results for the amplitude of v_S^{+1} and v_S^{-1} while ensuring an overall improved dynamic response of the detection system. This decoupling network is presented in the following section.

IV. Decoupling Signals in the DSRF

To introduce the decoupling network, one supposes a voltage vector consisting of two generic components rotating with $n\omega$ and $m\omega$ frequencies respectively, where m and n can be either positive or negative with ω the fundamental utility frequency. This voltage vector is shown in

$$\begin{aligned} v_{S\atop(\alpha\beta)} &= \begin{bmatrix}v_{S\alpha}\\ v_{S\beta}\end{bmatrix} \\ &= v^n_{S\atop(\alpha\beta)} + v^m_{S\atop(\alpha\beta)} \\ &= V_S^n\begin{bmatrix}\cos(n\omega t+\phi^n)\\ \sin(n\omega t+\phi^n)\end{bmatrix} + V_S^m\begin{bmatrix}\cos(m\omega t+\phi^m)\\ \sin(m\omega t+\phi^m)\end{bmatrix}. \end{aligned} \tag{9}$$

Additionally, two rotating reference frames are considered, dq^n and dq^m, whose angular positions are $n\hat{\theta}$ and $m\hat{\theta}$ respectively, where $\hat{\theta}$ is the phase angle detected by the PLL.

If a perfect synchronization of the PLL is possible, that is if $\hat{\theta}=\omega t$, the voltage vector in (9) can be expressed on the dq^n and dq^m reference frames as follows:

$$\begin{aligned} v_{S\atop(dq^n)} &= \begin{bmatrix}v_{Sd^n}\\ v_{Sq^n}\end{bmatrix} \\ &= V_S^n\begin{bmatrix}\cos(\phi^n)\\ \sin(\phi^n)\end{bmatrix} + V_S^m\cos(\phi^m)\begin{bmatrix}\cos((n-m)\omega t)\\ -\sin((n-m)\omega t)\end{bmatrix} \\ &\quad + V_S^m\sin(\phi^m)\begin{bmatrix}\sin((n-m)\omega t)\\ \cos((n-m)\omega t)\end{bmatrix} \end{aligned} \tag{10a}$$

$$\begin{aligned} v_{S\atop(dq^m)} &= \begin{bmatrix}v_{Sd^m}\\ v_{Sq^m}\end{bmatrix} \\ &= V_S^m\begin{bmatrix}\cos(\phi^m)\\ \sin(\phi^m)\end{bmatrix} + V_S^n\cos(\phi^n)\begin{bmatrix}\cos((n-m)\omega t)\\ \sin((n-m)\omega t)\end{bmatrix} \\ &\quad + V_S^n\sin(\phi^n)\begin{bmatrix}-\sin((n-m)\omega t)\\ \cos((n-m)\omega t)\end{bmatrix}. \end{aligned} \tag{10b}$$

In (10), the amplitude of the signal oscillation in the dq^n axes depends on the mean value of the signal in the dq^m axes, and vice versa. In order to cancel the oscillations in the dq^n axes signals, the decoupling cell shown in Fig. 5 is proposed. For cancelling out the oscillations in the dq^m axes signals, the same structure may be used but interchanging m and n in it.

Logically, for a correct operation of both decoupling cells it is necessary to design some mechanism to determine the value of $\overline{v}^n_{Sd}$, $\overline{v}^n_{Sq}$, $\overline{v}^m_{Sd}$ and $\overline{v}^m_{Sq}$. Keeping this goal in mind, the cross-feedback decoupling network shown in Fig. 6 is proposed. In this decoupling network the LPF block is a low-pass filter such as

$$LPF(s) = \frac{\omega_f}{s+\omega_f}. \tag{11}$$

For the analysis of the decoupling network depicted in Fig. 6 the following signals are defined:

$$u_1 = \cos((n-m)\omega t); \quad u_2 = \sin((n-m)\omega t). \tag{12}$$

Then, the following equations can be written:

$$\begin{aligned} \overline{V}_{Sd^n}(s) = \frac{\omega_f}{s+\omega_f}\big(&V_{Sd^n}(s) - U_1(s) * \overline{V}_{Sd^m}(s) \\ &- U_2(s) * \overline{V}_{Sq^m}(s)\big) \end{aligned} \tag{13a}$$

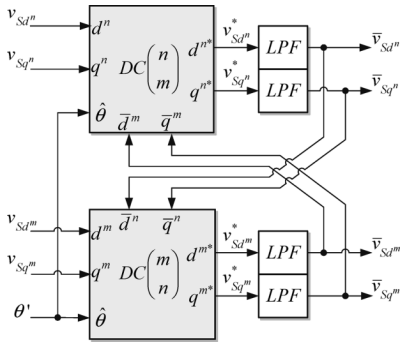

Fig. 6. Decoupling network of dq^n and dq^m reference frames.

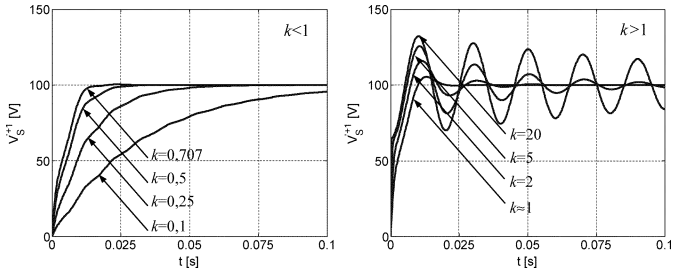

Fig. 7. Theoretical evolution of $\overline{v}_{Sd+1}$ for different values for k ($V_S^{+1} = 100$ V, $V_S^{-1} = 30$ V, $\omega = 2\pi 50$ rad/s).

$$\overline{V}_{Sq^n}(s) = \frac{\omega_f}{s+\omega_f}\left(V_{Sq^n}(s) - U_1(s) * \overline{V}_{Sq^m}(s) + U_2(s) * \overline{V}_{Sd^m}(s)\right) \quad (13b)$$

$$\overline{V}_{Sd^m}(s) = \frac{\omega_f}{s+\omega_f}\left(V_{Sd^m}(s) - U_1(s) * \overline{V}_{Sd^n}(s) + U_2(s) * \overline{V}_{Sq^n}(s)\right) \quad (13c)$$

$$\overline{V}_{Sq^m}(s) = \frac{\omega_f}{s+\omega_f}\left(V_{Sq^m}(s) - U_1(s) * \overline{V}_{Sq^n}(s) - U_2(s) * \overline{V}_{Sd^n}(s)\right) \quad (13d)$$

where $*$ represents the convolution product in the s-domain.

Transforming (13) into the time domain gives rise to the following expressions:

$$\dot{\overline{v}}_{Sd^n} = \omega_f(v_{Sd^n} - \overline{v}_{Sd^n} - u_1\overline{v}_{Sd^m} - u_2\overline{v}_{Sq^m}) \quad (14a)$$

$$\dot{\overline{v}}_{Sq^n} = \omega_f(v_{Sq^n} - \overline{v}_{Sq^n} - u_1\overline{v}_{Sq^m} + u_2\overline{v}_{Sd^m}) \quad (14b)$$

$$\dot{\overline{v}}_{Sd^m} = \omega_f(v_{Sd^m} - \overline{v}_{Sd^m} - u_1\overline{v}_{Sd^n} + u_2\overline{v}_{Sq^n}) \quad (14c)$$

$$\dot{\overline{v}}_{Sq^m} = \omega_f(v_{Sq^m} - \overline{v}_{Sq^m} - u_1\overline{v}_{Sq^n} - u_2\overline{v}_{Sd^n}). \quad (14d)$$

Finally, from (10), (12), and (14), the following state-space model may be written

$$\dot{x}(t) = A(t)\cdot x(t) + B(t)\cdot v(t)$$
$$y(t) = C\cdot x(t) \quad (15a)$$

where

$$x(t) = y(t) = \begin{bmatrix} \overline{v}_{Sd^n} \\ \overline{v}_{Sq^n} \\ \overline{v}_{Sd^m} \\ \overline{v}_{Sq^m} \end{bmatrix}; \quad v(t) = \begin{bmatrix} V_S^n\cos(\phi^n) \\ V_S^n\sin(\phi^n) \\ V_S^m\cos(\phi^m) \\ V_S^m\sin(\phi^m) \end{bmatrix}$$

$$A(t) = -B(t); \quad C = I \quad (15b)$$

and (15c), shown at the bottom of the page.

This state-space model corresponds to a multiple-input multiple-output linear time variant system. Since the analytic solution of this system is highly complex, its response will be solely evaluated considering $n = +1$ and $m = -1$, that is decoupling the positive and negative fundamental frequency components in the dq^{+1} and dq^{-1} axes. Additionally, in order to further simplify its solution, it will be considered that $\phi^{+1} = 0$ and $\phi^{-1} = 0$. Under such conditions, when $v(t)$ is suddenly applied in the form of a step-input expression (16) is obtained, which corresponds to the amplitude estimation of v_S^{+1}. In (16), the coefficient k is the ratio between the cut-off frequency of the LPF and the utility fundamental frequency ($k = \omega_f/\omega$)

$$\overline{v}_{Sd^{+1}} = V_S^{+1} - \left\{V_S^{+1}\cos(\omega t)\cos(\omega t\sqrt{1-k^2}) - \frac{1}{\sqrt{1-k^2}}\left(V_S^{+1}\sin(\omega t) - kV_S^{-1}\cos(\omega t)\right) \times \sin(\omega t\sqrt{1-k^2})\right\}e^{-k\omega t}. \quad (16)$$

The oscillatory terms in (16) decrease exponentially in time due to the term $e^{-k\omega t}$, therefore after a stabilization period defined by k the amplitude of v_S^{+1} may be finally determined. Fig. 7 shows expression (16) obtained for different values for k when $V_S^{+1} = 100$ V, $V_S^{-1} = 30$ V, and $\omega = 2\pi 50$ rad/s. As it can be observed, for $k \geq 1/\sqrt{2}$ the dynamic response becomes undamped. From these plots it seems reasonable to establish $k = 1/\sqrt{2}$, since the dynamic response is fast enough and does not exhibit oscillations in the amplitude estimation of v_S^{+1}.

It is worth to say that (16) comes from a particular analysis, where it is assumed that $\hat{\theta} = \omega t$. Taking into account that $\hat{\theta}$ is obtained by means of the PLL in the actual system, certain transient errors may appear in the dynamic response in relation to the theoretical response shown in Fig. 7. As shown in Fig. 7, as long as $k \leq 1/\sqrt{2}$, the higher the value assigned to k is the faster will be the speed of response. To increase the value of k beyond this limit would lead to higher transient errors, creating longer stabilization periods which could even give rise to instabilities in the detection system. There exists then a clear trade-off between dynamic response and stability, justifying why the value

$$B(t) = \omega_f \begin{bmatrix} 1 & 0 & \cos((n-m)\omega t) & \sin((n-m)\omega t) \\ 0 & 1 & -\sin((n-m)\omega t) & \cos((n-m)\omega t) \\ \cos((n-m)\omega t) & -\sin((n-m)\omega t) & 1 & 0 \\ \sin((n-m)\omega t) & \cos((n-m)\omega t) & 0 & 1 \end{bmatrix}. \quad (15c)$$

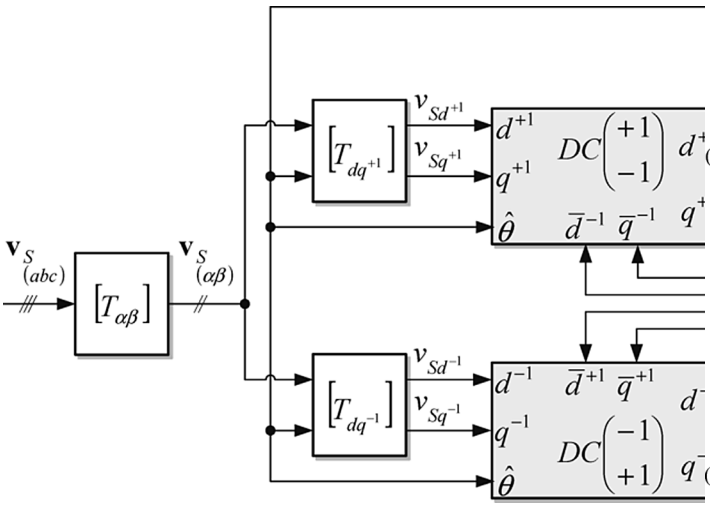

Fig. 8. Block diagram of the DDSRF–PLL.

of k is set to $1/\sqrt{2}$ in order to minimize oscillations and ensure the stability of the detection system.

As it will be shown in Section V, the above constraint in the maximum value of k is even more important when the utility voltages not only present unbalance at the fundamental frequency but also high order harmonics.

V. Structure and Behavior of the DDSRF-PLL

The block diagram of the DDSRF-PLL proposed in this paper is shown in Fig. 8. This PLL, as shown in the figure, is based on a conventional three-phase SRF-PLL structure [15]. Its performance improvement comes from the decoupling network added to the DSRF.

The decoupling network of the DDSRF-PLL cancels out the double frequency oscillations at 2ω in $v^*_{Sq^{+1}}$; therefore, there is no need to reduce the control loop bandwidth and the real amplitude of the positive sequence voltage component is indeed exactly detected.

To show the promising behavior of the proposed DDSRF-PLL, similar unbalanced grid operating conditions to those used to obtain the plots in Fig. 3 are considered in the following simulation, i.e., $V_S^{+1} = 100$ V, $V_S^{-1} = 30$ V $\phi^{+1} = \phi^{-1} = 0$ rad, and $\omega = 2\pi$ 50 rad/s. The plots of column (i) in Fig. 9 show the response of the DDSRF-PLL in presence of such unbalanced voltages when the control parameters are set to $k = 1/\sqrt{2}, k_p =$ 2,22 and $k_i =$ 246,7. The selection of k_p and k_i is based on the small-signal analysis reported in [17] and [18] and revised at the end of this section.

Fig. 9(b,i) and (9c,i) respectively show the detected phase angle, $\hat{\theta}$, and the detected amplitude, $\overline{v}_{Sd^{+1}} \equiv |\hat{v}_S^{+1}|$, for the positive sequence voltage component. Fig. 9(c,i) also shows the evolution of the signal at the input of the PLL controller, $v^*_{Sq^{+1}}$, which is free of oscillations at 2ω thanks to the action of the decoupling network. From the detected phase angle and amplitude, the positive sequence voltage can be readily reconstructed as shown in Fig. 9(d,i). This figure shows how the positive sequence component is in effect detected from zero initial conditions in less than one utility period. Fig. 9(c,i) on the other hand shows the response of the DDSRF-PLL in detecting the

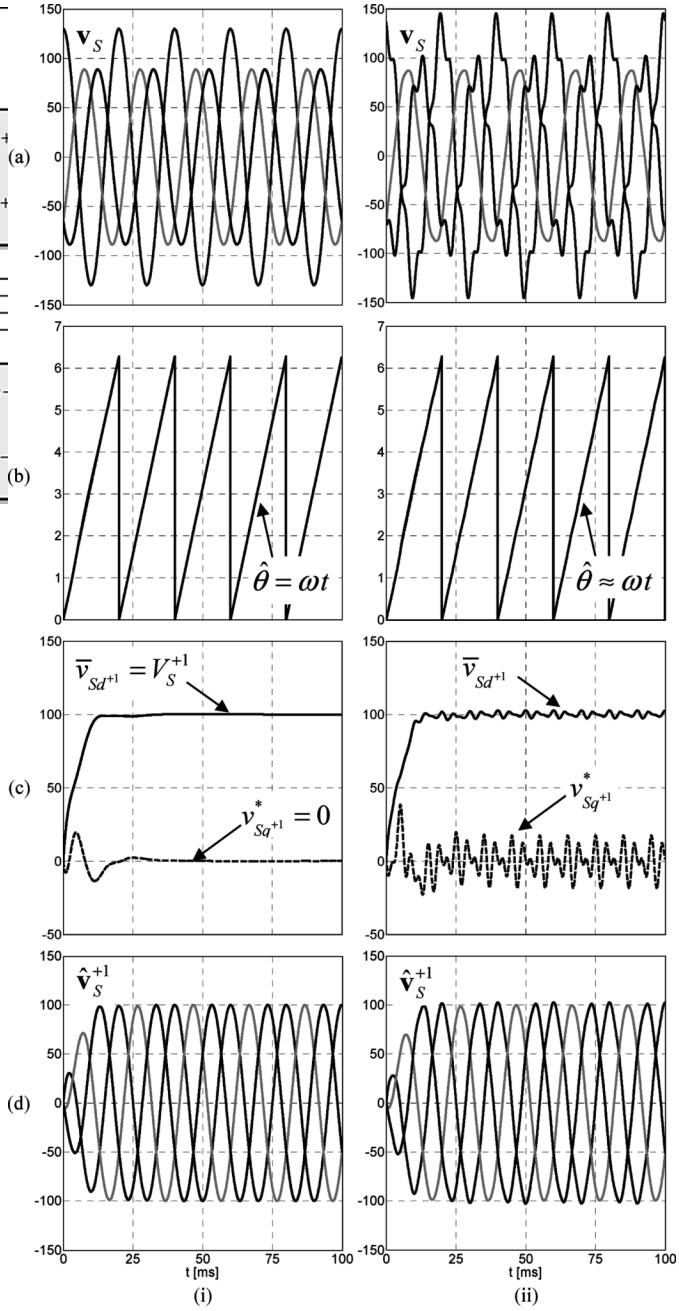

Fig. 9. Response of the DDSRF-PLL under (i) unbalanced and (ii) distorted grid operating conditions (a) utility voltage [V] (b) detected phase angle [rad], (c) DSRF axes voltage [V], (d) detected positive-sequence voltage [V].

amplitude of the positive sequence voltage component, closely resembling the results shown in Fig. 7 for $k =$0,707 which was obtained analytically. The slight differences between both figures are due to the fact that $\hat{\theta} \neq \omega t$ during the stabilization period of the DDSRF-PLL.

Comparing simulation results shown in the column (i) of Fig. 9 to those shown in Fig. 3 it is possible to state that the DDSRF-PLL completely eliminates the problems of the conventional SRF-PLL when the utility voltage is unbalanced [15], achieving higher performance than other systems designed with the same purpose [12]. In fact, even when considering a very improbable case in which the negative-sequence component

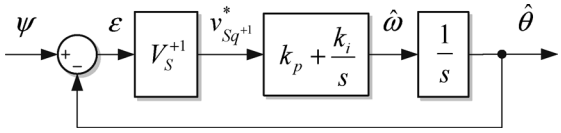

Fig. 10. Linearized control loop.

became as high as the positive one, the set of control parameters previously specified would ensure that the DDSRF-PLL perfectly synchronizes and detects the positive-sequence voltage without any steady-state error.

Regarding the presence of high-order harmonic distortion in the utility voltages, it was mentioned in Section II that the standard solution for SRF-PLL's is the reduction of its bandwidth seeking to minimize and reject the detrimental effect of the distorted voltages [15]. This solution however also reduces the system dynamics. In order to evaluate the behavior of the DDSRF-PLL when the utility voltage is strongly distorted, an unbalanced fifth harmonic component is added to the utility voltage. Fig. 9(a,ii) shows the unbalanced and distorted utility voltage characterized by $V_S^{+1} = 100$ V, $V_S^{-1} = 30$ V, $V_S^{+5} = 10$ V, and $V_S^{-5} = 10$ V. The plots of column (ii) in Fig. 9 show the simulation results of the DDSRF-PLL under such operating conditions. In this simulation, the control loop bandwidth is not reduced, thus use the control parameters specified earlier ($k = 1/\sqrt{2}$, $k_p = 2{,}22$ and $k_i = 246{,}7$). From Fig. 9(b,ii), it is worth noticing that the estimation of the phase angle of the positive-sequence voltage vector is quite accurate regardless of the distorted utility voltages. This characteristic is very interesting for control algorithms working on the dq synchronous reference frame. To explain why the error in the phase angle estimation is so low one can analyze the signal $v_{Sq^{+1}}$ when the system is in steady-state, that is when $\hat{\theta} \approx \omega t$. In such a case

$$v_{Sq^{+1}} \approx V_S^{+1}(\omega t - \hat{\theta}) + V_S^{-1}\sin(-2\omega t + \phi^{-1}) + V_S^{+5}\sin(4\omega t + \phi^{+5}) + V_S^{-5}\sin(-6\omega t + \phi^{-5}). \quad (17)$$

Since the decoupling network canceled out the effect of the negative-sequence component, the decoupled signal $v^*_{Sq^{+1}}$ is simply given by

$$v^*_{Sq^{+1}} \approx V_S^{+1}(\omega t - \hat{\theta}) + V_S^{+5}\sin(4\omega t + \phi^{+5}) + V_S^{-5}\sin(-6\omega t + \phi^{-5}). \quad (18)$$

As Fig. 8 shows, $v^*_{Sq^{+1}}$ is applied to the input of the PI controller and later integrated in order to obtain $\hat{\theta}$. Consequently, the linearized control loop of Fig. 10 can be obtained as shown below [17], [18]

$$\psi = \omega t + \frac{V_S^{+5}}{V_S^{+1}}\sin(4\omega t + \phi^{+5}) + \frac{V_S^{-5}}{V_S^{+1}}\sin(-6\omega t + \phi^{-5}) = \omega t + \tilde{\psi}. \quad (19)$$

The transfer function of this control diagram is

$$P(s) = \frac{\hat{\theta}}{\psi}(s) = \frac{2\xi\omega_c s + \omega_c^2}{s^2 + 2\xi\omega_c s + \omega_c^2} \quad (20)$$

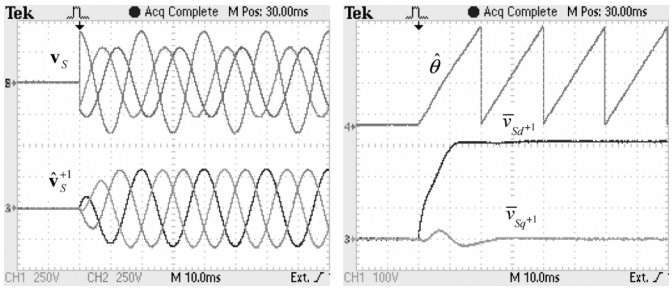

Fig. 11. Characteristic waveforms at the start up of the DDSRF–PLL.

where

$$\omega_c = \sqrt{V_S^{+1}k_i}, \quad \xi = \frac{k_p}{2}\sqrt{\frac{V_S^{+1}}{k_i}}. \quad (21)$$

The oscillatory term in (19), $\tilde{\psi}$, acts as a disturbance to the PLL. Fortunately, $\tilde{\psi}$ has a relatively low amplitude because its harmonic components are divided by the positive-sequence component amplitude, V_S^{+1}. The effect of this small disturbance on the detected angle is further attenuated as a consequence of the low-pass characteristic of $P(s)$. According to the values given to k_p and k_i, (21) indicates that the parameters of $P(s)$ are set approximately equal to $\omega_c = 2\pi$ 25 rad/s and $\xi = 1/\sqrt{2}$, which implies that high-order harmonics in $\tilde{\psi}$ will have almost not effect on the detected phase angle $\hat{\theta}$.

Further, assuming that $\hat{\theta} = \omega t$, the decoupled signal $v^*_{Sd^{+1}}$ is given by

$$v^*_{Sd^{+1}} \approx V_S^{+1} + V_S^{+5}\cos(4\omega t + \phi^{+5}) + V_S^{-5}\cos(-6\omega t + \phi^{-5}). \quad (22)$$

The amplitude of the positive-sequence is detected by filtering the signal of (22) through the low pass filter described by (11); therefore, the calculation of the error incurred in when estimating the amplitude of the positive-sequence component is quite straightforward. Obviously, the lower is the cut-off frequency of the filter and the higher is its order, the higher will be the attenuation of the oscillatory terms of $v^*_{Sd^{+1}}$. This fact justifies once more the constraint of Section IV about the maximum value for k. However, it is necessary to recall that a small value of k, although it would make the detection system very robust, would give rise to too slow a transient response, which could not be acceptable for many an application.

VI. Experimental Results

In order to verify the simulation results, the scenario previously simulated has been implemented using an ELGAR SM5250A programmable ac source and a DSpace DS1103 DSP board as control system. For the first experiment, the values for the different parameters were kept equal to those used earlier in the waveforms shown in Fig. 9. For the implementation of the DDSRF-PLL algorithm on the DSP, the sampling time used was 50 μS. Fig. 11 shows the results obtained, clearly resembling the waveforms obtained through simulation. This result was expected since the sampling period used was significantly smaller than the time constant of the system. Fig. 11 also depicts signal $\overline{v}_{Sq^{+1}}$, which after the

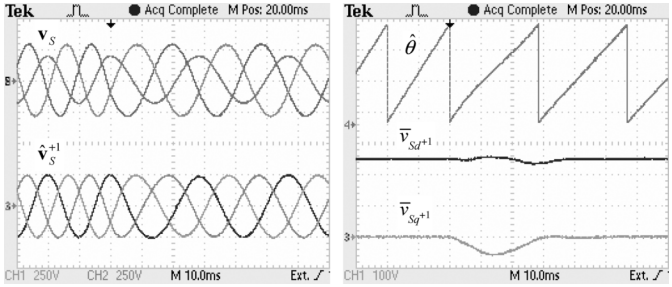

Fig. 12. Characteristic waveforms when the utility frequency varies.

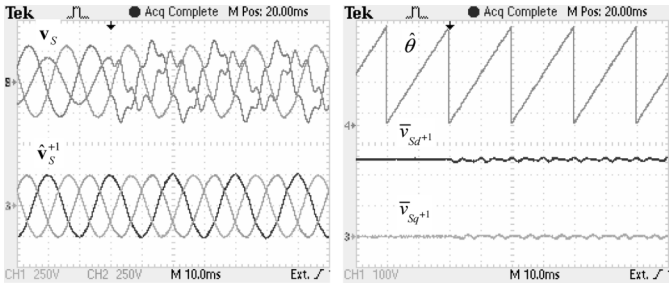

Fig. 13. Characteristic waveforms when the utility voltage is distorted.

stabilization period (approximately one grid cycle) becomes zero.

One of the most important features offered by PLL-based structures respect to other techniques is their capability to adapt to changes in the utility frequency. In order to test this feature in the DDSRF-PLL, the value of constant k was reduced to $k = 1/2$ thus increasing the damping in the system response. All the other parameters were kept as in the previous experiment. Fig. 12 depicts the behavior of the proposed DDSRF-PLL when the utility frequency suddenly changes from 50 Hz to 35 Hz. This frequency decrement of 30% is twice as high as the maximum admissible variation per the EN-50160 standard for isolated networks. These waveforms show how the DDSRF-PLL attained good results when subjected to this frequency change even under unbalanced conditions. This is naturally a highly desirable feature for the control of power electronics systems applied to wind generators [2], especially when these generators work in island mode or are connected to weak grids.

In order to experimentally evaluate the behavior of the DDSRF-PLL when the utility voltage is unbalanced and distorted, a utility voltage characterized by $V_S^{+1} = 80$ V, $V_S^{-1} = 20$ V, $V_S^{+5} = 10$ V, and $V_S^{-5} = 10$ V was programmed in the ac source.

The waveforms shown in Fig. 13 were obtained with the same parameters used in the previous case. In this figure it is possible to appreciate how, even setting $k = 1/2$, there exist slight oscillations in $\overline{v}_{Sd^{+1}}$ due to the distorted voltages, which in turn slightly distort the reconstructed fundamental-frequency positive-sequence component [see Fig. 13(b)]. Although these results are not entirely satisfactory, it should be kept in mind that the actual utility voltage is usually less distorted than the one considered in this experiment [19]. As mentioned in Section V, a possible way to improve this response nonetheless would be the reduction of the PLL bandwidth, or alternatively to increase the order of the low pass filters. These measures would naturally reduce the dynamic response of the system.

It is also worth mentioning that the higher the order of the harmonics in the utility voltage the lower will be the effect over the detected signals, so notches and glitches have almost no effect over the DSRF-PLL output.

VII. Conclusion

The study and results presented in this paper showed that the proposed DDSRF–PLL is a suitable solution to the detection of fundamental-frequency positive-sequence component of unbalanced and distorted utility voltages. The proposed method exploited a dual synchronous reference frame voltage characterization, adding a decoupling network to a standard three-phase PLL in order to effectively separate the positive- and negative-sequence voltage components in a fast and accurate way. Simulations together with a complete experimental evaluation were presented in order to verify and validate the excellent results obtained by the proposed DDSRF–PLL.

References

[1] M. Cichowlas, M. Malinowski, D. L. Sobczuk, M. P. Kazmierkowski, P. Rodríguez, and J. Pou, "Active, filtering function of three-phase PWM boost rectifier under different line voltage conditions," *IEEE Trans. Ind. Electron.*, vol. 52, no. 2, pp. 410–419, Apr. 2005.

[2] R. Teodorescu and F. Blaabjerg, "Flexible control of small wind turbines with grid failure detection operating in stand-alone and grid-connected mode," *IEEE Trans. Power Electron.*, vol. 19, no. 5, pp. 1323–1332, Sep. 2004.

[3] J. G. Nielsen, M. Newman, H. Nielsen, and F. Blaabjerg, "Control and testing of a dynamic voltage restorer (DVR) at medium voltage level," *IEEE Trans. Power Electron.*, vol. 19, no. 3, pp. 806–813, May 2004.

[4] M. H. Haque, "Power flow control and voltage stability limit: regulating transformer versus UPFC," *Proc. Inst. Elect. Eng.*, vol. 151, pp. 299–304, May 2004.

[5] P. Mattavelli, "A close-loop selective harmonic compensation for active filters," *IEEE Trans. Ind. Appl.*, vol. 37, no. 1, pp. 81–89, Jan./Feb. 2001.

[6] A. Ghosh and A. Joshi, "A new algorithm for the generation of reference voltages of a DVR using the method of instantaneous symmetrical components," *IEEE Power Eng. Rev.*, vol. 22, no. 1, pp. 63–65, Jan. 2002.

[7] J. Svensson, "Synchronisation methods for grid-connected voltage source converters," *Proc. Inst. Elect. Eng.*, vol. 148, pp. 229–235, May 2001.

[8] H. Song, H. Park, and K. Nam, "An instantaneous phase angle detection algorithm under unbalanced line voltage condition," in *Proc. IEEE Power Electron. Spec. Conf*, 1999, vol. 1, pp. 533–537.

[9] H. Song and K. Nam, "Instantaneous phase-angle estimation algorithm under unbalanced voltage-sag conditions," *Proc. Inst. Elect. Eng.*, vol. 147, pp. 409–415, Nov. 2000.

[10] V. Kaura and V. Blasco, "Operation of a phase locked loop system under distorted utility conditions," *IEEE Trans. Ind. Appl.*, vol. 33, no. 1, pp. 58–63, Jan./Feb. 1997.

[11] M. Aredes and L. F. C. Monteiro, "A control strategy for shunt active filter," in *Proc. IEEE Int. Conf. Harm. Power Quality*, Oct. 2002, vol. 2, pp. 472–477.

[12] S. M. Silva, B. M. Lopes, B. J. C. Filho, R. P. Campana, and W. C. Boaventura, "Performance evaluation of PLL algorithms for single-phase grid-connected systems," in *Proc. IEEE Ind. Appl. Conf.*, 2004, vol. 4, pp. 2259–2263.

[13] M. Karimi-Ghartemani, H. Karimi, and M. R. Iravani, "A magnitude/phase-locked loop system based on estimation of frequency and in-phase/quadrature-phase amplitudes," *IEEE Trans. Ind. Electron*, vol. 51, no. 2, pp. 511–517, Apr. 2004.

[14] M. Karimi-Ghartemani and M. R. Iravani, "A method for synchronization of power electronic converters in polluted and variable-frequency environments," *IEEE Trans. Power Syst.*, vol. 19, no. 3, pp. 1263–1270, Aug. 2004.

[15] M. Karimi-Ghartemani, M. R. Iravani, and F. Katiraei, "Extraction of signals for harmonics, reactive current and network-unbalance compensation," *Proc. Inst. Elect. Eng.*, vol. 152, pp. 137–143, Jan. 2005.

[16] S. Chung, "A phase tracking system for three phase utility interface inverters," *IEEE Trans. Power Electron.*, vol. 15, no. 3, pp. 431–438, May 2000.
[17] P. Rodríguez, J. Bergas, and J. A. Gallardo, "A new positive sequence voltage detector for unbalanced power systems," in *Proc. Eur. Conf. Power Electron. Appl.*, Sep. 2002, [CD ROM].
[18] P. Rodriguez, L. Sainz, and J. Bergas, "Synchronous double reference frame PLL applied to a unified power quality conditioner," in *Proc. IEEE Int. Conf. Harm. Power Quality*, Oct. 2002, vol. 2, pp. 614–619.
[19] J. Wikston, "Limits for low voltage ($<$1 kV) buses," in *Proc. IEEE Power Eng. Soc. Summer Meeting*, Jul. 2001, vol. 2, pp. 801–803.

Pedro Rodríguez (S'99–M'04) received the B.S. degree in electrical engineering from the University of Granada, Granada, Spain, in 1989and the M.S. and Ph.D. degrees in electrical engineering from the Technical University of Catalonia (UPC), Terrassa, Spain, in 1994 and 2004, respectively.

In 1990, he joined the faculty of UPC as an Assistant Professor. He became an Associate Professor in 1993. He stayed as a Researcher in the Center for Power Electronics Systems CPES, at Virginia Polytechnic Institute and State University, Blacksburg, and in the Institute of Energy Technology IET, Aalborg University, Aalborg, Denmark, in 2005 and 2006. He is a member of the Power Quality and Renewable Energy (QuPER) Research Group, UPC. His research interests include power conditioning, integration of distributed energy systems, and control of power converters.

Josep Pou (S'97–M'03) received the B.S., M.S., and Ph.D. degrees in electrical engineering from the Technical University of Catalonia (UPC), Terrassa, Spain, in 1989, 1996, and 2002, respectively.

During 1989, he was the Technical Director of Polylux S.A. In 1990, he joined the faculty of UPC as an Assistant Professor. He became an Associate Professor in 1993. From February 2001 to January 2002, and from February 2005 to January 2006, he was a Researcher in the Center for Power Electronics Systems, Virginia Polytechnic Institute and State University (Virginia Tech), Blacksburg. He is a member of the Power Quality and Renewable Energy (QuPER) Research Group. He has authored more than 50 published technical papers and has been involved in several industrial projects and educational programs in the fields of power electronics and systems. His research interests include modeling and control of power converters, multilevel converters, power quality, renewable energy systems, and motor drives.

Joan Bergas (M'97) was born in Manresa, Spain, in 1970. He received the B.S. degree in industrial engineering and the Ph.D. degree in engineering from the Universitat Politècnica de Catalunya, Barcelona, Spain, in 1992 and 2000, respectively.

Since 2002, he has been Assistant Professor in the Electrical Engineering Department, Universitat Politècnica de Catalunya. His research interest lies in the areas of power system quality, power electronics, and digital motor control.

J. Ignacio Candela (S'99–M'04) was born in Bilbao, Spain, in 1962. He received the B.S. degree in industrial engineering from the Universitat Politècnica de Catalunya, Barcelona, Spain, in 2000.

Since 1991, he has been Professor in the Electrical Engineering Department, Universitat Politècnica de Catalunya. His main field of research is power quality and electrical machines.

Rolando P. Burgos (S'96–M'03) received the B.S., M.S., and Ph.D. degrees in electronic engineering from the University of Concepción, Concepción, Chile, in 1994, 1997, 1999, and 2002, respectively.

In 2002, he joined as a Postdoctoral Fellow the NSF Engineering Research Center for Power Electronics Systems CPES, Virginia Polytechnic Institute and State University, Blacksburg, where he is currently a Research Assistant Professor. His area of interest is the modeling, control, and synthesis of power electronics conversion systems for more electric aircraft and marine applications.

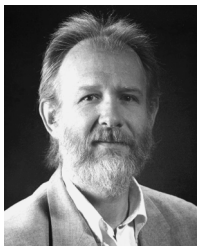

Dushan Boroyevich (F'06) received the B.S. degree from the University of Belgrade, Yugoslavia, in 1976, the M.S. degree from the University of Novi Sad, Yugoslavia, in 1982, and the Ph.D. degree from the Virginia Polytechnic Institute and State University (Virginia Tech), Blacksburg, in 1986.

From 1986 to 1990, he was an Assistant Professor and Director of the Power and Industrial Electronics Research Program, Institute for Power and Electronic Engineering, University of Novi Sad, and later, acting head of the Institute. He then joined the Bradley Department of Electrical and Computer Engineering, Virginia Tech, as Associate Professor. He is now the American Electric Power Professor at the Department and co-Director of the NSF Engineering Research Center for Power Electronics Systems (CPES). His research interests include multiphase power conversion, power electronics systems modeling and control, and multidisciplinary design optimization.

Dr. Boroyevich is a Member of Phi Kappa Phi, the IEEE Power Electronics Society AdCom, and the IEEE Industry Applications Society Industrial Power Converter Committee.